Applied Physics Letters

Far-field thermal radiation from short-pitch silicon-carbide nanopillar arrays

Cite as: Appl. Phys. Lett. **121**, 131702 (2022); https://doi.org/10.1063/5.0109819
Submitted: 14 July 2022 • Accepted: 13 September 2022 • Published Online: 27 September 2022

Ramin Pouria, Philippe K. Chow, Tom Tiwald, et al.

AIP Publishing

Applied Physics Letters ARTICLE scitation.org/journal/apl

Far-field thermal radiation from short-pitch silicon-carbide nanopillar arrays

Cite as: Appl. Phys. Lett. **121**, 131702 (2022); doi: 10.1063/5.0109819
Submitted: 14 July 2022 · Accepted: 13 September 2022 ·
Published Online: 27 September 2022

Ramin Pouria,[1,2,a] Philippe K. Chow,[3] Tom Tiwald,[4] Saman Zare,[1,2] and Sheila Edalatpour[1,2,a]

AFFILIATIONS

[1]Department of Mechanical Engineering, University of Maine, Orono, Maine 04469, USA
[2]Frontier Institute for Research in Sensor Technologies, University of Maine, Orono, Maine 04469, USA
[3]Columbia Nano Initiative, Columbia University, New York, New York 10027, USA
[4]Applications Engineering Group, J.A. Woollam Company, Lincoln, Nebraska 68508, USA

Note: This paper is part of the APL Special Collection on Thermal Radiation at the Nanoscale and Applications.
[a]**Authors to whom correspondence should be addressed:** ramin.pouria@maine.edu and sheila.edalatpour@maine.edu

ABSTRACT

Silicon carbide (SiC) supports surface phonons in the infrared region of the electromagnetic spectrum where these modes can be thermally emitted. Additionally, the magnitude, spectrum, and direction of thermal radiation from SiC can be controlled by engineering this material at the sub-wavelength scale. For these reasons, SiC nanopillars are of high interest for thermal-radiation tuning. So far, theoretical and experimental studies of thermal emission from SiC nanopillars have been limited to long-pitch arrays with a microscale interpillar spacing. It is not clear how far-field thermal emission from SiC nanopillars is affected when the interparticle spacing reduces to the nanometer scale, where the near-field interaction between adjacent nanopillars arises and the array becomes zero order. In this Letter, we study physical mechanisms of far-field thermal radiation from zero-order arrays of silicon-carbide nanopillars with a nanoscale interpillar spacing. We show that the increased volume of thermal emitters and thermal radiation of the hybrid waveguide-surface-phonon-polariton mode from zero-order arrays increase the spectral emissivity of silicon carbide to values as large as 1 for a wide range of angles. The enhanced, dispersion-less thermal emission from a zero-order SiC array of nano-frustums with an optimized interspacing of 300 nm is experimentally demonstrated. Our study provides insight into thermal radiation from dense nanostructures and has significant implications for thermal management of electronic devices and energy harvesting applications.

Flat surfaces of polar dielectric materials can support propagating surface phonon polaritons (SPhPs) in the infrared range of the electromagnetic spectrum, where these modes can be thermally emitted.[1–3] The spectral location of the SPhP modes is between the longitudinal and transverse optical phonon frequencies of the material, which is referred to as the reststrahlen band.[3,4] The parallel component of the wavevector, k_ρ, for the SPhPs is greater than the wavevector in both the dielectric material and the free space (k_0). As such, the SPhPs are evanescent in both media.[2] Since SPhPs are confined to a distance approximately equal to the thermal wavelength from the emitter, they can only contribute to the near-field thermal radiation. Indeed, polar dielectrics are poor far-field emitters in their reststrahlen band, since these materials have negative permittivity (and thus, are highly reflective) in this band.[4] One- and two-dimensional periodic gratings have been proposed for enhancing the far-field thermal emission from polar dielectric materials.[5–12] Gratings reduce k_ρ of SPhPs to values less than k_0, such that the SPhPs can couple to propagating modes in the free space.[5–12] The coupling of SPhPs to propagating modes significantly enhances the far-field thermal emission characterized by the emissivity of the material. However, the far-field thermal emission from gratings is highly coherent and, thus, directional.[5–12] Sub-wavelength particles of polar dielectric materials can support localized surface phonons (LSPhs).[4,13–19] Unlike SPhPs, LSPhs can have k_ρs smaller than k_0 and, thus, can contribute to the far-field thermal radiation. Additionally, the dispersion relation of LSPhs is almost flat,[16] such that LSPhs can enhance emissivity in a wide range of directions. When fabricated on a polar dielectric substrate, an array of sub-wavelength particles can also serve as a grating and couple SPhPs of the substrate to the far zone. This coupling provides an additional mechanism for enhancing emissivity of the material. Due to the enhanced emissivity and the ability to tune the spectrum and direction of thermal radiation, sub-wavelength structures of polaritonic materials, such as silicon carbide (SiC), have

been of high interest.[20–25] More complex structures made of sub-wavelength particles of two different geometries have also proven promising for achieving near-perfect absorption in a broad band.[26] So far, most of the theoretical and experimental studies on thermal radiation from SiC sub-wavelength structures have been concerned with diffractive arrays that have a pitch size, Λ, greater than half of the thermal wavelength, λ. The mechanism of thermal radiation in diffractive arrays is different from short-pitch, non-diffractive (zero-order) arrays with $\Lambda < \frac{\lambda}{2}$. This Letter addresses the emissivity of zero-order arrays of sub-wavelength particles of SiC both theoretically and experimentally. It is shown that while zero-order arrays cannot couple the SPhPs emitted from the substrate into the far zone, they can emit a dispersion-less electromagnetic mode, namely, the hybrid waveguide-SPhP resonance. This electromagnetic mode causes a new peak in thermal radiation from the array. Additionally, the effect of interpillar spacing on the emissivity of periodic arrays of SiC nanoparticles is addressed in this Letter. While the emissivity of the array initially increases by decreasing the interpillar spacing (due to the increase in the volume of the thermal emitter), further decrease in interpillar spacing reduces thermal emission due to the strong near-field interactions between the nanoparticles. It is demonstrated that the increased volume of emitters and thermal radiation of the waveguide-SPhP mode in the zero-order arrays can be capitalized for increasing the spectral emissivity significantly up to the blackbody value of 1 in a wide range of directions. The enhanced far-field thermal radiation from nanopillars has significant implications for applications such as high-temperature SiC electronic cooling and energy harvesting using thermophotovoltaic devices.

To study the effect of interparticle spacing on far-field thermal radiation, we select 6H-SiC nanopillars with the shape of a frustum of a cone [see the inset of Fig. 1(b)]. The frustums have a bottom diameter of $D_1 = 700$ nm, a top diameter of $D_2 = 500$ nm, and a height of $H = 1000$ nm. The dimensions of the nanopillars are selected such that they emit both longitudinal and transversal LSPhs, while they can also be experimentally fabricated. Thermal emission by isolated nanopillars is proportional to the imaginary part of their electric polarizability, $\mathrm{Im}[\alpha]$ (see Sec. 1 of the supplementary material). As such, the spectral locations of the longitudinal and transversal LSPhs can be estimated by considering the spectrum of $\mathrm{Im}[\alpha]$. For cylindrical nanopillars, the polarizability along the direction j ($j = x, y, z$) is found as $\alpha_j = V\frac{\varepsilon-1}{1+L_j(\varepsilon-1)}$, where V, ε, and L_j are the volume, dielectric function, and depolarization factor of the nanopillar in the direction j, respectively.[25,26] The depolarization factor of the cylindrical nanopillars along x, y, and z directions [see the inset of Fig. 1(a)] can be estimated as $L_x = L_y = \frac{1}{2}\cos\varphi - i\frac{k_0^3}{6\pi}V$ and $L_z = 1 - \cos\varphi - \frac{k_0^2}{6\pi}VC_z - i\frac{k_0^3}{6\pi}V$, where i is the imaginary unit, $\varphi = \tan^{-1}(D/H)$, and $C_z = \frac{3}{2H}\ln\left|\frac{1+E}{1-E}\right|$ with $E = 1 + \left(\frac{D}{H}\right)^2$.[27,28] For nano-frustums, the diameter varies along the z-axis from 500 nm at the top to 700 nm at the bottom. The spectral locations of the longitudinal and transversal LSPhs of a frustum-shaped nanopillar can be estimated by considering $\mathrm{Im}[\alpha]$ of cylindrical nanopillars with diameters between 500 and 700 nm. Figure 1(a) shows $\mathrm{Im}[\alpha_{x,y}]$ (transversal polarizability) and $\mathrm{Im}[\alpha_z]$ (longitudinal polarizability) for cylinders of height $H = 1000$ nm and three diameters D of 500, 600, and 700 nm. A temperature T of 400 °C is assumed, and the ordinary and extraordinary dielectric functions of 6H-SiC at this temperature are measured using ellipsometry (see Sec. S2 of the supplementary material). The ordinary dielectric function of 6H–SiC was used for the calculations. As it is seen from Fig. 1(a), $\mathrm{Im}[\alpha_{x,y}]$ and $\mathrm{Im}[\alpha_z]$ each has a peak corresponding to the transversal and longitudinal dipolar LSPhs, respectively. When D changes from 500 to 700 nm, the spectral location of the longitudinal peak varies from 894 to 918 cm^{-1} while the wavenumber of the transversal mode decreases very slightly from 934 to 930 cm^{-1}. Figure 1(b) shows the normalized absorption cross section for an isolated frustum-shaped nanopillar at $T = 400$ °C as obtained using the SCUFF-SCATTER tool of the SCUFF-EM electromagnetic solver.[29,30] The peak and the shoulder at 905 and 911 cm^{-1} are within the spectral band in which $\mathrm{Im}[\alpha_z]$ is maximal, and thus, they are due to excitation of the longitudinal LSPhs. The peak at 933 cm^{-1} is associated with the resonance of $\mathrm{Im}[\alpha_{x,y}]$ caused by excitation of transversal dipolar LSPhs. Next, thermal emission from an array of nanopillars with an interpillar spacing, d, is studied. The spectral, directional emissivity of a free-standing array of nanopillars with a square lattice [see the inset of Fig. 1(c)] at $T = 400$ °C is simulated for various d ranging from 2300 to 50 nm. The spectral, directional emissivity, ε'_η, is found from the field amplitude reflection and transmission coefficients as $\varepsilon'_\eta = \frac{1}{2}\sum_{\gamma=\mathrm{TE,TM}}\left(1 - \left|R_\eta^\gamma\right|^2 - \left|T_\eta^\gamma\right|^2\right)$, where η refers to the wavenumber, γ shows the polarization state (TE and TM stand for the transverse electric and magnetic polarizations, respectively), and R_η^γ and T_η^γ are the reflection and transmission coefficients, respectively.[31] The terms R_η^γ and T_η^γ are simulated using the SCUFF-TRANSMISSION module of the SCUFF-EM electromagnetic solver.[30,32] Figure 1(c) shows the spectral, normal emissivity of the nanopillar array for the considered interpillar spacing. The longitudinal and transversal dipolar LSPhs of the isolated nanopillars are observed in the emissivity spectrum of the array for all considered interspacing values. When $d = 2300$ nm, the electromagnetic interactions of neighboring nanopillars are weak and the spectral locations of the longitudinal and transversal LSPhs (906, 912, and 933 cm^{-1}) are almost the same as those for isolated nanopillars. The emissivity of the array for $d = 2300$ nm is very low ($\varepsilon'_{\eta,\max} \sim 0.2$). As d decreases, the emissivity of the array significantly enhances in a non-monotonic manner. The emissivity increases as d decreases to ~150 nm, and then, it decreases when d is further reduced to 50 nm. The non-monotonic variation of the emissivity with d can be explained by considering that there are two competing effects on the far-field thermal emission as d decreases. On the one hand, the emitting volume per unit surface area of the array increases, but on the other hand, the dipole moments of the emitters decrease due to the near-field interactions between the nanopillars. As it is seen from Eq. (S3) of the supplementary material, the emitted energy from a nanopillar is proportional to its dipole moment. The dipole moment of nanopillar i of the array, $\mathbf{p}_i$, can qualitatively be approximated as[33]

$$\mathbf{p}_i = \alpha_i\left(\frac{\mathbf{p}_i^{fl}}{\varepsilon_0 V(\varepsilon-1)} + \frac{k_0^2}{\varepsilon_0}\sum_{j\neq i}\bar{\bar{\mathbf{G}}}_{ij}\cdot\mathbf{p}_j\right), \quad (1)$$

where $\mathbf{p}_i^{fl}$ is the thermally fluctuating dipole moment of the nanopillars, ε_0 is the permittivity of the free space, and $\bar{\bar{\mathbf{G}}}_{ij}$ is the free space electric Green's function between nanopillars i and j.[33] In Eq. (1), the sum of the two terms in the parentheses indicates the total electric field in the nanopillar i. The first term is the thermal field of the nanopillar, while the second term represents the electric field generated at

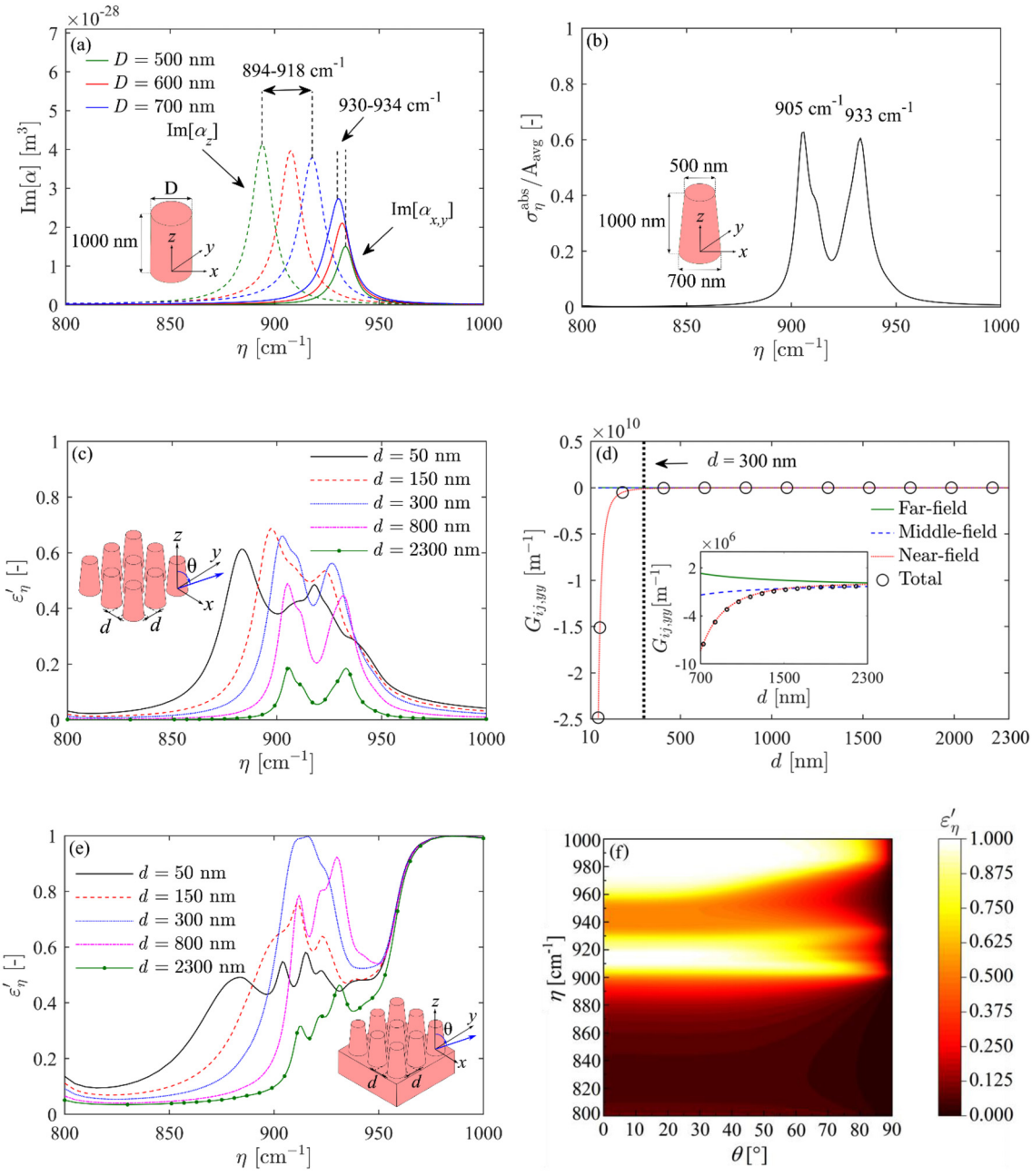

FIG. 1. (a) The imaginary part of the longitudinal and transversal polarizability of 6H–SiC cylindrical nanopillars for three diameters of 500, 600, and 700 nm. (b) The absorption cross section for a frustum-shaped nanopillar normalized by a circular cross section with an average diameter of 600 nm. (c) The spectral, normal emissivity for a free-standing array of 6H–SiC frustum-shaped nanopillars. (d) The real part of the *yy* componet of the free space Green's function between two points *i* and *j* separated by a distance *d* along the *y* axis. (e) The spectral, normal emissivity of a 6H–SiC frustum-shaped nanopillar array on a 6H–SiC substrate. (f) A color plot of the spectral, directional emissivity of the on-substrate array of 6H–SiC frustum-shaped nanopillars, as shown in Fig. 1(e), with $d = 300$ nm.

nanopillar i due to emission from all other nanopillars of the array. Equation (1) shows that the interactions between the nanopillars, which is represented by the free space Green's function $\bar{\bar{\mathbf{G}}}_{ij}$, affect the dipole moments of the nanopillars, $\mathbf{p}_i$. The free space Green's function can be decomposed into three far-field, middle-field, and near-field components (see Sec. S3 of the supplementary material).[34] As an example, these three components for the real part of $G_{ij,yy}$ are shown vs d in Fig. 1(d) at $\eta = 903\ \mathrm{cm}^{-1}$. It is seen that at $d = 2300$ nm, $G_{ij,yy}$ is mostly dominated by the middle-field contribution. As d decreases, the absolute values of the far-field, middle-field, and near-field

components increase as $\frac{1}{d}$, $\frac{1}{d^2}$, and $\frac{1}{d^3}$, respectively (see Sec. S3 of the supplementary material). The enhancement of the near-field component with decreasing d is much stronger than that for the middle and far fields, such that $G_{ij,yy}$ is totally dominated by the near-field contribution when $d < 1400$ nm. Figure 1(d) also shows that the near-field interactions between nanopillars are very significant when $d \lesssim 300$ nm. The initial enhancement of the emissivity with decreasing d from 2300 to ~150 nm is driven by the increase in the volume of the emitters. As d decreases further to 50 nm, the strong near-field interactions reduce $\mathbf{p}_i$ and, thus, the emissivity of the array. The spectral locations of the LSPh peaks do not shift significantly when d reduces to ~300 nm. However, when $d < 300$ nm, the LSPh peaks redshift due to the strong near-field interactions of the nanopillars.

The emissivity of the array can be enhanced further by exploiting thermal emission of the SPhPs from a SiC substrate on which the nanopillar array can be fabricated. As mentioned before, the SPhPs are evanescent in the free space and, thus, do not contribute to the far-field thermal emission. At a given wavenumber, the parallel component of the wavevector for the SPhP modes is determined from the dispersion relation as $k_\rho^{\mathrm{SPhP}} = k_0\sqrt{\frac{\varepsilon}{\varepsilon+1}}$.[2] When a shallow grating is added to a flat SiC surface, k_ρ^{SPhP} is modified as $k_{\rho,mn}^{\mathrm{SPhP}} = k_\rho^{\mathrm{SPhP}} \pm m\frac{2\pi}{\Lambda} \pm n\frac{2\pi}{\Lambda}$, where m and n are integers.[8] For long-pitch arrays with $\Lambda > \frac{\lambda}{2}$, $k_{\rho,mn}^{\mathrm{SPhP}}$ can reduce to values below k_0 and, thus, the SPhP modes can become propagative in certain directions in the free space.[8] Short-pitch shallow gratings with $\Lambda < \frac{\lambda}{2}$, which are zero order, cannot sufficiently reduce $k_{\rho,m}^{\mathrm{SPhP}}$ to below k_0 (see Sec. S4 of the supplementary material). However, when zero-order gratings are deep, a broad gap appears in the photonic structure of the material, and a new, dispersion-less electromagnetic mode emerges within this bandgap.[35,36] This new electromagnetic mode, referred to as the hybrid waveguide-SPhP resonance,[35,36] corresponds to highly localized electromagnetic field in the narrow spaces between nanopillars and results in a new peak in far-field thermal radiation. Unlike SPhP modes coupled to the free space using long-pitch gratings, the dispersion-less waveguide-SPhP mode enhances thermal emission in all directions which is beneficial for thermal management applications. Figure 1(e) shows the spectral, normal emissivity for on-substrate SiC arrays. The additional peak observed in the emissivity spectrum corresponds to thermal emission of the hybrid waveguide-SPhP mode. The dipole moments of the nanopillars are also affected in the presence of the electric field thermally radiated from the substrate, $\mathbf{E}^{\mathrm{sub}}$. The substrate field $\mathbf{E}^{\mathrm{sub}}$ should be added to the terms in the parentheses in Eq. (1) when using this equation for analyzing the dipole moments of the on-substrate arrays. The existence of $\mathbf{E}^{\mathrm{sub}}$ in Eq. (1) can modify the spectrum and magnitude of the dipole moments. As a result, the LSPh peaks of the on-substrate array are redshifted relative to the ones of the free-standing array. As d decreases, the waveguide-SPhP mode redshifts toward the longitudinal LSPhs. When $d = 300$ nm, the spectral overlap of these two modes results in the blackbody thermal emission ($\varepsilon'_\eta \sim 1$) from the array in the spectral band of 910–916 cm^{-1}. As it was mentioned before, the enhancement of emissivity is not directional. Figure 1(f) shows a color plot of ε'_η for the array with $d = 300$ nm. It is seen that the designed array has significantly high thermal emission in a spectral band spanning several wavelengths and for angles as large as 75° from the surface normal. The non-directional thermal emission from the array, which is also observed for smaller interpillar spacing of $d = 50$ nm, is due to dispersion-less nature of the LSPh and waveguide-SPhP modes.

To experimentally demonstrate enhanced far-field thermal radiation from short-pitch arrays, the spectral, directional emissivity of an array of 6H–SiC frustum-shaped nanopillars with an interpillar spacing of $d = 300$ nm is measured. The nanopillars are fabricated on a 1×1 cm^2 surface area of a 430-μm-thick 6H–SiC substrate. The nanopillars are defined on the substrate using inductively coupled plasma reactive ion etching (ICP-RIE). An array of patterned chromium circles is used as an etch hard mask, which is defined using electron beam lithography (fabrication details in Sec. S5 of the supplementary material). The erosion of the chromium mask in the radial direction during the etching process causes a frustum, rather than the cylindrical shape for the nanopillars. A scanning electron microscope (SEM) image and a brightfield microscope image of the fabricated sample are shown in Figs. 2(a) and 2(b), respectively. A setup for measuring emissivity is also established [Fig. 2(c)]. In this setup, the sample is mounted on an aluminum stage using a nickel based metal adhesive (Durabond, 952FS). The stage holds a cartridge heater (Watlow Firerod) inside, and it is assembled on a rotary stage (Standa, Inc., 8MR174-11-20) which is used for directional measurements. The sample is heated up to 400 °C. The temperature of the sample is determined by knowing that the emissivity of SiC at the Christiansen wavenumber (990.1 cm^{-1}) is 1.[8] Thermal emission by the heated sample ($I_{S\eta}$) is directed toward a Fourier Transform Infrared (FTIR) spectrometer (Thermo Fisher Scientific, Nicolet iS50) equipped with a mercury-cadmium-telluride detector (Thermo Fisher Scientific, MCT-A/CdTe) using flat (Thorlabs, PFSQ20-03-M03) and parabolic (Thorlabs, MPD269-M03) mirrors. An iris is placed in front of the sample to limit the collection angle. Thermal emission by a blackbody (ISDC, IR-563) located at the same optical path toward the FTIR spectrometer as the sample is also collected ($I_{BB,\eta}$). The background thermal radiation ($I_{E,\eta}$) is recorded when both the heater and the blackbody are turned off, and it is subtracted from the sample and blackbody emissions. Finally, the spectral, directional emissivity is found as $\varepsilon'_\eta = \frac{(I_{S,\eta} - I_{E,\eta})}{(I_{BB,\eta} - I_{E,\eta})}$. Figure 3(a) shows the measured emissivity for the fabricated sample at $\theta = 0$ to 60° with respect to the surface normal. As it was predicted by numerical simulations, the sample shows modest angular dependence. The normal emissivity measured for a bare SiC substrate is also shown in Fig. 3(a) for comparison. The presence of the array on the substrate increases the total (spectrally integrated), normal emissivity in the spectral band of 800–980 cm^{-1} more than 100% without diminishing the large emissivity of the substrate between 980 and 1000 cm^{-1}. It is seen that the measured emissivity is slightly lower than those theoretically predicted in Fig. 1(e). Additionally, the theoretical large-emissivity band in Fig. 1(e) is split into two distinct peaks in the measurements, and the peaks are shifted relative to the simulations (911 and 916 cm^{-1} are predicted theoretically, while 902 and 923 cm^{-1} are measured). This difference is attributed to the surface damage during the ICP-RIE[14] as well as the difference between the fabricated and modeled geometries. The SEM images of the fabricated sample show non-uniformity in the shape and spacing of the nanopillars as well as the presence of a trench around the nanopillars [see Fig. 2(a)]. As it is seen from Fig. 1(e), the emissivity of the array drops below 1 with decreasing and increasing d from 300 nm. The splitting and shifts of the peaks are mostly due to the

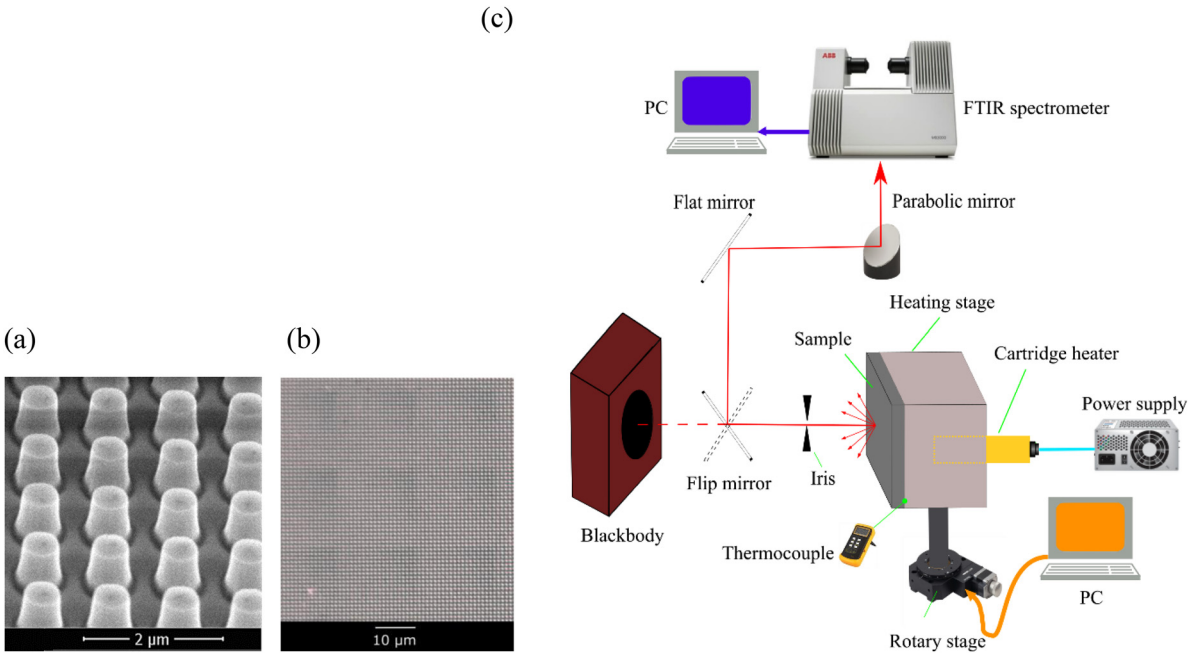

FIG. 2. (a) An SEM image and (b) a brightfield microscope image of the fabricated 6H–SiC nanopillar array. (c) A schematic of the setup established for measuring the spectral, directional emissivity.

existence of the trench. Figure 3(b) shows the predicted emissivity in the presence of a conical trench of height and width 50 nm around the nanopillars. The splitting of the large-emissivity band into two peaks is theoretically predicted, and the simulated wavenumbers of the peaks in the presence of the trench (906 and 921 cm^{-1}) are close to the experimentally measured values (902 and 923 cm^{-1}).

To summarize, the physics underlying the far-field thermal emission from zero-order arrays of SiC nanopillars was theoretically and experimentally studied. It was shown that reducing the interpillar spacing in an array of 6H–SiC nanopillars to the nanometer scale increases the emissivity due to the increase in the volume of thermal emitters. However, when the interpillar spacing is reduced below ~300 nm, the near-field interactions between the nanopillars reduce their dipole moments and eventually cause a drop in the emissivity despite the increased emitting volume. It was also demonstrated that the array can be engineered such that the LSPhs emitted by the nanopillars spectrally overlap the waveguide-SPhP resonance of the array resulting in blackbody emission in a spectral region in the reststrahlen band. Our study unveils the physical mechanisms of far-field thermal radiation from zero-order nanostructures of polaritonic materials and demonstrates that nanoengineering surface phonons provide a great opportunity for increasing the far-field thermal emission.

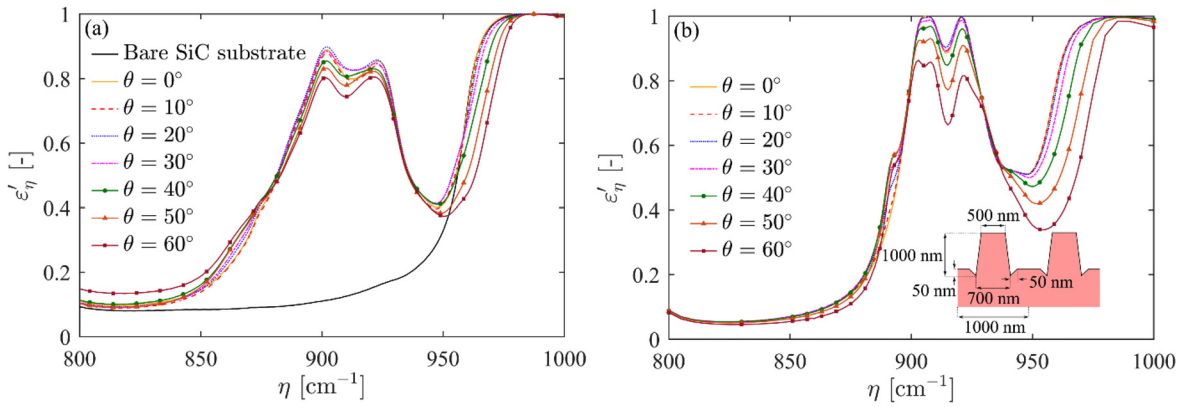

FIG. 3. (a) The spectral, directional emissivity experimentally measured for the nanopillar array shown in Fig. 3(a). (b) The theoretically predicted spectral, directional emissivity for the nanopillar array shown in Fig. 1(e) and in the presence of a trench around the nanopillars.

See the supplementary material for the following information: the derivation of thermal radiation from a cylindrical dipole; the details of ellipsometry measurement of the dielectric function of 6H–SiC at 400 °C; the far-, middle-, and near-field components of the free space Green's function; the details of the fabrication method for SiC nanopillars; and isofrequency contours of surface phonon polaritons for short- and long-pitch shallow gratings.

This work was financially supported by the National Science Foundation under Grant No. CBET-1804360. The authors thank Stephen Abbadessa for his assistance with implementing the experimental setup for measuring emissivity.

AUTHOR DECLARATIONS

Conflict of Interest

The authors have no conflicts to disclose.

Author Contributions

Ramin Pouria: Data curation (lead); Formal analysis (equal); Methodology (lead); Validation (lead); Visualization (lead); Writing – original draft (equal). **Philippe K. Chow:** Methodology (supporting); Writing – original draft (supporting). **Tom E. Tiwald:** Methodology (supporting); Writing – original draft (supporting). **Saman Zare:** Methodology (supporting); Writing – review & editing (supporting). **Sheila Edalatpour:** Conceptualization (lead); Formal analysis (equal); Funding acquisition (lead); Methodology (supporting); Supervision (lead); Writing – original draft (equal).

DATA AVAILABILITY

The data that support the findings of this study are available within the article and its supplementary material.

REFERENCES

[1]Z. M. Zhang, *Nano/Microscale Heat Transfer*, 1st ed. (McGraw-Hill Nanoscience and Technology, 2007).
[2]K. Joulain, J.-P. Mulet, F. Marquier, R. Carminati, and J.-J. Greffet, "Surface electromagnetic waves thermally excited: Radiative heat transfer, coherence properties and Casimir forces revisited in the near field," Surf. Sci. Rep. **57**(3), 59–112 (2005).
[3]S. Foteinopoulou, G. C. R. Devarapu, G. S. Subramania, S. Krishna, and D. Wasserman, "Phonon-polaritonics: Enabling powerful capabilities for infrared photonics," Nanophotonics **8**(12), 2129–2175 (2019).
[4]J. D. Caldwell, L. Lindsay, V. Giannini, I. Vurgaftman, T. L. Reinecke, S. A. Maier, and O. J. Glembocki, "Low-loss, infrared and terahertz nanophotonics using surface phonon polaritons," Nanophotonics **4**(1), 44–68 (2015).
[5]J. Le Gall, M. Olivier, and J.-J. Greffet, "Experimental and theoretical study of reflection and coherent thermal emission by a SiC grating supporting a surface-phonon polariton," Phys. Rev. B **55**(15), 10105 (1997).
[6]J.-J. Greffet, R. Carminati, K. Joulain, J.-P. Mulet, S. Mainguy, and Y. Chen, "Coherent emission of light by thermal sources," Nature **416**(6876), 61–64 (2002).
[7]N. Dahan, A. Niv, G. Biener, Y. Gorodetski, V. Kleiner, and E. Hasman, "Enhanced coherency of thermal emission: Beyond the limitation imposed by delocalized surface waves," Phys. Rev. B **76**(4), 045427 (2007).
[8]C. Arnold, F. Marquier, M. Garin, F. Pardo, S. Collin, N. Bardou, J.-L. Pelouard, and J.-J. Greffet, "Coherent thermal infrared emission by two-dimensional silicon carbide gratings," Phys. Rev. B **86**(3), 035316 (2012).
[9]E. Hasman, V. Kleiner, N. Dahan, Y. Gorodetski, K. Frischwasser, and I. Balin, "Manipulation of thermal emission by use of micro and nanoscale structures," J. Heat Transfer **134**(3), 031023 (2012).
[10]A. Hervé, J. Drévillon, Y. Ezzahri, K. Joulain, D. D. S. Meneses, and J.-P. Hugonin, "Temperature dependence of a microstructured SiC coherent thermal source," J. Quant. Spectrosc. Radiat. Transfer **180**, 29–38 (2016).
[11]H. Chalabi, A. Alù, and M. L. Brongersma, "Focused thermal emission from a nanostructured SiC surface," Phys. Rev. B **94**(9), 094307 (2016).
[12]R. Starko-Bowes, J. Dai, W. Newman, S. Molesky, L. Qi, A. Satija, Y. Tsui, M. Gupta, R. Fedosejevs, and S. Pramanik, "Dual-band quasi-coherent radiative thermal source," J. Quant. Spectrosc. Radiat. Transfer **216**, 99–104 (2018).
[13]J. D. Caldwell, O. J. Glembocki, Y. Francescato, N. Sharac, V. Giannini, F. J. Bezares, J. P. Long, J. C. Owrutsky, I. Vurgaftman, and J. G. Tischler, "Low-loss, extreme subdiffraction photon confinement via silicon carbide localized surface phonon polariton resonators," Nano Lett. **13**(8), 3690–3697 (2013).
[14]Y. Chen, Y. Francescato, J. D. Caldwell, V. Giannini, T. W. W. Maß, O. J. Glembocki, F. J. Bezares, T. Taubner, R. Kasica, and M. Hong, "Spectral tuning of localized surface phonon polariton resonators for low-loss mid-IR applications," ACS Photonics **1**(8), 718–724 (2014).
[15]I. Razdolski, Y. Chen, A. J. Giles, S. Gewinner, W. Schöllkopf, M. Hong, M. Wolf, V. Giannini, J. D. Caldwell, and S. A. Maier, "Resonant enhancement of second-harmonic generation in the mid-infrared using localized surface phonon polaritons in subdiffractional nanostructures," Nano Lett. **16**(11), 6954–6959 (2016).
[16]C. R. Gubbin, F. Martini, A. Politi, S. A. Maier, and S. de Liberato, "Strong and coherent coupling between localized and propagating phonon polaritons," Phys. Rev. Lett. **116**(24), 246402 (2016).
[17]C. R. Gubbin, S. A. Maier, and S. de Liberato, "Theoretical investigation of phonon polaritons in SiC micropillar resonators," Phys. Rev. B **95**(3), 035313 (2017).
[18]C. R. Gubbin, R. Berte, M. A. Meeker, A. J. Giles, C. T. Ellis, J. G. Tischler, V. D. Wheeler, S. A. Maier, J. D. Caldwell, and S. de Liberato, "Hybrid longitudinal-transverse phonon polaritons," Nat. Commun. **10**(1), 1682 (2019).
[19]G. Lu, C. R. Gubbin, J. R. Nolen, T. G. Folland, K. Diaz-Granados, I. I. Kravchenko, J. A. Spencer, M. J. Tadjer, O. J. Glembocki, S. de Liberato, and J. D. Caldwell, "Collective phonon–polaritonic modes in silicon carbide subarrays," ACS Nano **16**, 963 (2022).
[20]J. A. Schuller, T. Taubner, and M. L. Brongersma, "Optical antenna thermal emitters," Nat. Photonics **3**(11), 658–661 (2009).
[21]T. Wang, P. Li, D. N. Chigrin, A. J. Giles, F. J. Bezares, O. J. Glembocki, J. D. Caldwell, and T. Taubner, "Phonon-polaritonic bowtie nanoantennas: Controlling infrared thermal radiation at the nanoscale," ACS Photonics **4**(7), 1753–1760 (2017).
[22]B. Neuner III, C. Wu, G. T. Eyck, M. Sinclair, I. Brener, and G. Shvets, "Efficient Infrared thermal emitters based on low-albedo polaritonic metasurfaces," Appl. Phys. Lett. **102**(21), 211111 (2013).
[23]G. Lu, C. R. Gubbin, J. R. Nolen, T. Folland, M. J. Tadjer, S. de Liberato, and J. D. Caldwell, "Engineering the spectral and spatial dispersion of thermal emission via polariton–phonon strong coupling," Nano Lett. **21**(4), 1831–1838 (2021).
[24]G. Lu, J. R. Nolen, T. G. Folland, M. J. Tadjer, D. G. Walker, and J. D. Caldwell, "Narrowband polaritonic thermal emitters driven by waste heat," ACS Omega **5**(19), 10900–10908 (2020).
[25]S. Enoch and N. Bonod, *Plasmonics: From Basics to Advanced Topics* 1st ed. (Springer, 2012).
[26]D. Chen, J. Dong, J. Yang, Y. Hua, G. Li, C. Guo, C. Xie, M. Liu, and Q. Liu, "Realization of near-perfect absorption in the whole reststrahlen band of SiC," Nanoscale **10**(20), 9450–9454 (2018).
[27]A. O. Silva and J. C. W. A. Costa, "Retrieving the effective permittivity of an optical metamaterial structured with metallic cylindrical nanorods an analytical approach based on the calculation of the depolarization field," J. Microwaves, Optoelectron. Electromagn. Appl. **13**(1), 10–28 (2014).
[28]S. Zare, R. Pouria, and S. Edalatpour, "Validity of the effective medium theory for modeling near-field thermal emission by nanowire arrays," J. Quant. Spectrosc. Radiat. Transfer **261**, 107482 (2021).
[29]M. T. H. Reid and S. G. Johnson, see http://homerreid.github.io/scuff-em-documentation/applications/scuff-scatter/scuff-scatter/ for "Solving electromagnetic scattering problems with Scuff-Scatter."

[30]M. T. H. Reid and S. G. Johnson, "Efficient computation of power, force, and torque in BEM scattering calculations," IEEE Trans. Antennas Propag. **63**(8), 3588–3598 (2015).
[31]S. Edalatpour and M. Francoeur, "Size effect on the emissivity of thin films," J. Quant. Spectrosc. Radiat. Transfer **118**, 75–85 (2013).
[32]M. T. H. Reid and S. G. Johnson, see http://homerreid.github.io/scuff-em-documentation/tests/FresnelScattering/FresnelScattering/ for "Fresnel scattering."
[33]S. Edalatpour, M. Čuma, T. Trueax, R. Backman, and M. Francoeur, "Convergence analysis of the thermal discrete dipole approximation," Phys. Rev. E **91**(6), 063307 (2015).
[34]H. F. Arnoldus, "Representation of the near-field, middle-field, and far-field electromagnetic green's functions in reciprocal space," J. Opt. Soc. Am. B **18**(4), 547–555 (2001).
[35]F. J. Garcia-Vidal, J. Sanchez-Dehesa, A. Dechelette, E. Bustarret, T. Lopez-Rios, T. Fournier, and B. Pannetier, "Localized surface plasmons in lamellar metallic gratings," J. Lightwave Technol. **17**(11), 2191 (1999).
[36]I. R. Hooper and J. R. Sambles, "Dispersion of surface plasmon polaritons on short-pitch metal gratings," Phys. Rev. B **65**(16), 165432 (2002).